FOCUS ON:

Overview of Dynamic Contrast-Enhanced MRI in Prostate Cancer Diagnosis and Management

Sadhna Verma[1]
Baris Turkbey[2]
Naira Muradyan[3]
Arumugam Rajesh[4]
Francois Cornud[5]
Masoom A. Haider[6]
Peter L. Choyke[2]
Mukesh Harisinghani[7]

[1]Department of Radiology, University of Cincinnati Medical Center, 234 Goodman St, PO Box 670761, Cincinnati, OH 45267-0761. Address correspondence to S. Verma (drsadhnaverma@gmail.com).

[2]The Molecular Imaging Program, National Cancer Institute, National Institutes of Health, Bethesda, MD.

[3]iCAD, Inc, Nashua, NH.

[4]University Hospitals of Leicester NHS Trust, Leicester General Hospital, Leicester, United Kingdom.

[5]Hôpital Cochin, Paris, France.

[6]Department of Radiology, University of Toronto, and University Health Network, Toronto, ON, Canada.

[7]Department of Radiology, Massachusetts General Hospital, Harvard Medical School, Boston, MA.

OBJECTIVE. This article is a primer on the technical aspects of performing a high-quality dynamic contrast-enhanced MRI (DCE-MRI) examination of the prostate gland.

CONCLUSION. DCE-MRI is emerging as a useful clinical technique as part of a multiparametric approach for evaluating the extent of primary and recurrent prostate cancer. Performing a high-quality DCE-MRI examination requires a good understanding of the technical aspects and limitations of image acquisition and postprocessing techniques.

P rostate cancer is a commonly diagnosed tumor in men that represents a broad spectrum of severity, ranging from indolent to highly lethal [1]. The use of prostate-specific antigen (PSA) serum screening has increased the diagnosis of prostate cancer. Prostate cancers are composed of both indolent and more aggressive cancers. The earlier diagnosis of aggressive cancers may account for a recent reduction in prostate cancer–specific death rates.

One problem with the current standard of care is that elevated PSA values inevitably lead to random prostate biopsies, which, in turn, lead to the discovery of incidental, often inconsequential, tumors [2]. Meanwhile, these same random biopsies may miss significant disease. Thus, MRI may play a role in conjunction with PSA for localizing biopsy sites and identifying those tumors more likely to cause death if left untreated.

The current MRI evaluation consists of one or more anatomic and functional techniques, such as T2-weighted MRI, diffusion-weighted MRI (DWI), MR spectroscopic imaging (MRSI), and dynamic contrast-enhanced MRI (DCE-MRI). Therefore, the current standard is to perform a multiparametric prostate MRI examination, recognizing that no single MRI sequence is sufficient to characterize prostate cancer. Each of the functional MR components has clinical advantages and limitations, and the optimal combination of anatomic and functional MR sequences still needs to be established.

However, DCE-MRI has become an important component of the multiparametric strategy and is emerging as a useful clinical technique for evaluating the severity, location, and extent of primary and recurrent prostate cancer. This technique differs from other functional MRI techniques in that it uses an exogenous contrast agent (low-molecular-weight gadolinium chelate) to assess tumor angiogenesis. The purpose of this article is to provide a detailed summary of efforts to date in prostate DCE-MRI as well as to present a guide for performing DCE-MRI in patients with known or suspected prostate cancer.

Prostate Cancer Angiogenesis

Like many tumors in other organs, prostate cancer shows earlier and more pronounced enhancement than surrounding normal prostate tissue on DCE-MRI [3]. This enhancement pattern is thought to be related to tumor angiogenesis. More aggressive tumors have the ability to initiate an angiogenic "switch" that upregulates molecular pathways, leading to the production and release of angiogenic factors, such as the vascular permeability factor or vascular endothelial growth factor. As a result, the number of vessels increases, and these newly formed tumor vessels have higher permeability than do normal vessels because of weak integrity of the vessel wall [4–6]. In general, tumor vessels are more permeable than normal vessels, more heterogeneous in size, and more disorganized. Studies suggest that the prognosis worsens as the
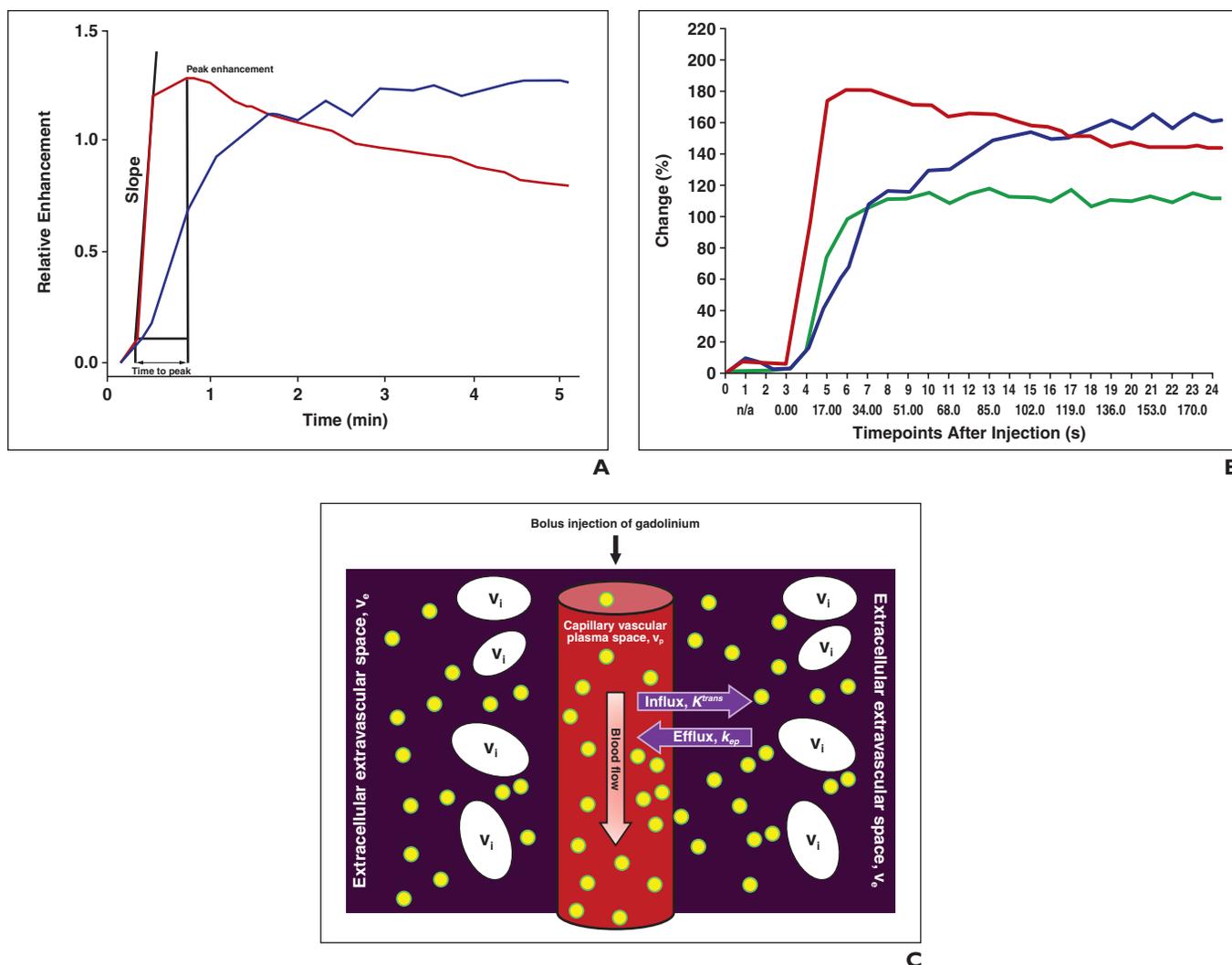
Fig. 1—Semiquantitative and quantitative parameters for dynamic contrast-enhanced MRI (DCE-MRI) analysis.
A, Chart shows semiquantitative parameters. Time-signal intensity curves from DCE-MRI show faster and stronger enhancement and faster washout in prostate cancer *(red)* than in healthy prostate tissue (*blue*). Commonly used semiquantitative parameters are derived from enhancement-time curve: onset time, slope of first-pass curve, time to peak, peak enhancement, and washout.
B, Chart shows differentiation of three patterns of washout phase: type 1 (*blue*), progressive (enhancement increases over time); type 2 (*green*), plateau (no change in enhancement over time); and type 3 (*red*), wash-out (early faster enhancement followed by decreasing enhancement over time).
C, Diagram shows quantitative parameters and method for calculating pharmacokinetic parameters using four-compartment model devised by Tofts et al [24]. These compartments are usually expressed as fractions of tissue volume. Where v_e is fractional extracellular space, v_p is fraction occupied by plasma, and v_i is fraction occupied by intracellular space. Low-molecular-weight contrast agent (*yellow dots*) distributes exclusively in intravascular blood plasma and in extravascular extracellular space. Pharmacokinetic parameters listed are K^{trans} and k_{ep}. Transfer constant, K^{trans}, describes diffusion of intravascular contrast medium into extracellular space. When distribution in body and renal elimination cause contrast medium concentration in plasma to drop below that in extracellular space, contrast medium from extracellular space diffuses back into plasma, which is described by rate constant, k_{ep}. K^{trans} [min^{-1}] = permeability surface area product per unit volume of tissue, k_{ep} [min^{-1}] = efflux rate constant, v_p = fractional plasma volume, $v_e = K^{trans}/k_{ep}$ = extracellular-extravascular volume fraction.

number of abnormal vessels in prostate cancer increases [7, 8]. For instance, it has been shown that microvessel density, which is established by immunohistochemistry on pathologic specimens, is an independent predictor of pathologic stage and often correlates with DCE-MRI results [9]. These histologic observations have prompted an interest in DCE-MRI for the noninvasive assessment of prostate cancer.

Dynamic Contrast-Enhanced MRI: Principles and Technique

The term "dynamic" is derived from the multiple serial images that are collected after injection of contrast media. The clinical application of DCE-MRI for prostate cancer is based on data showing that malignant lesions show earlier and faster enhancement and earlier contrast agent washout compared with healthy prostate tissues [10, 11] (Fig. 1). This requires fast bolus administration of contrast media combined with rapid acquisition methods.

DCE-MRI requires the use of serial 3D acquisitions before, during, and after a bolus of low-molecular-weight gadolinium contrast media, typically via the antecubital vein, using an injection rate of 2–4 mL/s followed by a 20-mL saline flush. IV-injected contrast agents pass from the arteries to the tissue microvasculature and extravasate within seconds

TABLE 1: Summary of Dynamic Contrast-Enhanced MRI Protocols

Vendor	TR/TE (ms)	Flip Angle (°)	FOV (cm)	Acquisition Matrix Resolution (mm)	Reconstruction Matrix Resolution (mm)	No. of Slices	Thickness (mm)	Temporal Resolution (s)	No. of Phases
GE Healthcare (3 T)	4.6/1.4	15	24	256/0.93	512/0.46	38	3	5.8[a]	48
GE Healthcare (1.5 T)	4.5/1.6	15	22	160/1.375	256/0.86	26	4	18	21
Philips Healthcare (3 T)	3.65/2.3	9	26.2	$188 \times 96/1.4 \times 2.7$	256/1.02	20	3	5.6	54
Siemens Healthcare (1.5 T)	4.9/1.8	10	18	128/1.4	256/0.7[b]	20	3.5	8.5	35

Note—Examinations performed using endorectal coil. Optimal slice thickness is 3 mm for diagnostic imaging at both 1.5 T and 3 T with maximal thickness of 4 mm. Dynamic contrast-enhanced acquisition should be continued for at least 5 minutes to detect optimal washout.
[a]Keyhole approach used during image acquisition.
[b]Keyhole technique used during postprocessing with true 256 × 256 resolution. Mask dataset acquired before contrast injection.
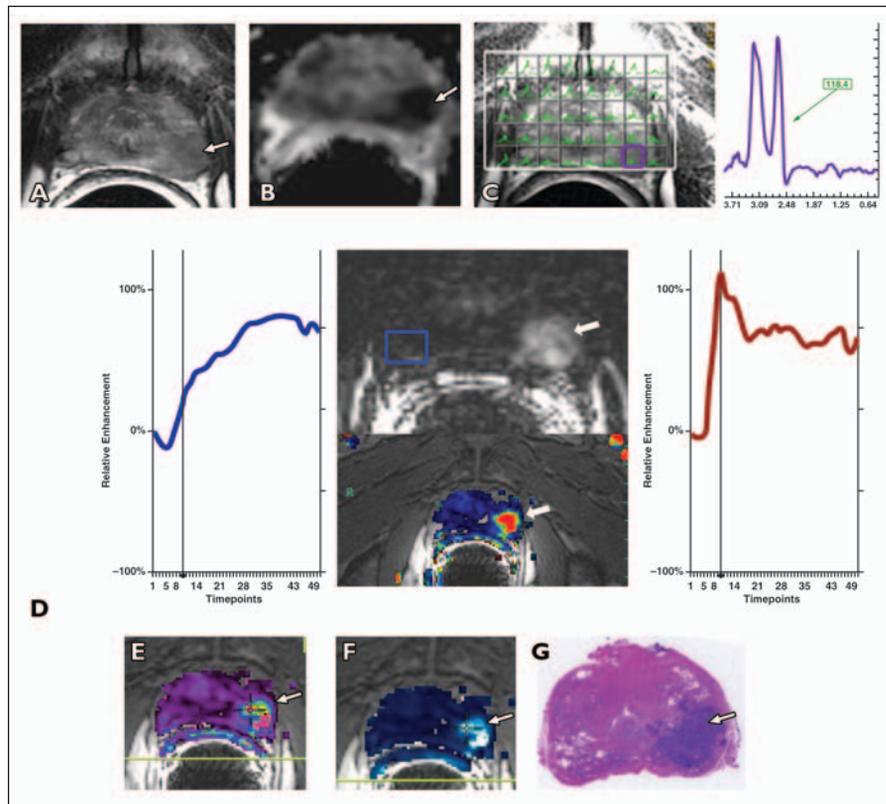

Fig. 2—Typical multiparametric prostate MRI examination in 56-year-old man with prostate-specific antigen level of 4.5 ng/mL and histologically proven prostate cancer with Gleason score of 7 (3 + 4), biopsied 8 weeks before staging MRI. Patient underwent nerve-sparing radical prostatectomy after staging MRI.
A, Axial T2-weighted image shows low-signal-intensity mass in left midgland to apex peripheral zone (*arrow*) and normal right peripheral zone.
B, Apparent diffusion coefficient (ADC) map shows restricted diffusion in low-signal mass (*arrow*) (measured ADC of carcinoma = 0.72×10^{-3} mm^2/s).
C, MR spectroscopy image overlying T2-weighted axial image shows high ch + cr / ci (choline + creatine / citrate) ratio (*purple voxel*) corresponding to low-signal-intensity mass. MR spectrum from tumor shows high choline (cho) peak at 3.2 ppm that is above that of citrate (ci) at 2.64 ppm. cho + cr / ci = 1.42, where cr = creatine; this value is typical of prostate cancer.
D, Contrast-enhanced images are overlaid on T2-weighted MR image and plot of relative contrast enhancement in both regions of interest over time is obtained. Early contrast-enhanced T1-weighted gradient-recalled echo image at peak enhancement and color map (wash-in and washout) show avid enhancement in left midgland peripheral zone mass (*arrows*). Healthy peripheral zone tissue is marked by blue square. Prostate cancer (*red*) shows earlier onset time, shorter time to peak, and higher peak enhancement than normal peripheral zone tissue. Prostate cancer also shows early washout of contrast material after maximum enhancement is reached, whereas healthy peripheral zone tissue (*blue*) shows enhancement plateau during acquisition period (5.8 s/timepoint).
E and **F,** Fusion of transverse T2-weighted image with color-encoded K^{trans} (forward volume transfer constant) map (**E**) and fusion of transverse T2-weighted image with color-encoded k_{ep} (reverse reflux rate constant) map (**F**) delineate tumor area (*arrow*).
G, Photomicrograph from prostatectomy specimen shows cancer in left midgland peripheral zone (*arrow*).

to the extravascular extracellular space. Extracellular space is also called the "leakage space." Contrast agents in vessels and in the extracellular space shorten local relaxation times, leading to a rapid brightening of signal on T1-weighted sequences. Of course, the ability to measure vessel leakiness is in part related to blood flow (i.e., it is difficult to identify leakiness if the flow is too low). Thus, the signal measured on DCE-MRI represents a combination of perfusion and permeability. A fast injection rate of the contrast agent captured with fast 3D acquisitions ensures that early enhancement within prostate tumors relative to background will be detected. DCE-MRI is sensitive to alterations in vascular permeability, extracellular space, and blood flow.

Image Acquisition

Dynamic contrast-enhancement techniques typically use 3D T1-weighted fast spoiled gradient-echo MRI sequences to repeatedly image a volume of interest after the administration of a bolus of IV contrast agent. T1-weighted spoiled gradient-echo sequences provide high sensitivity to T1 changes, high signal-to-noise ratios, adequate anatomic coverage, and rapid data acquisition. Typically, 3D image sets are obtained sequentially every few seconds for up to 5–10 minutes. Ideally, the acquisitions should be obtained approximately every 5 seconds to allow the detection of early enhancement; however, many centers use acquisition times up to 10 seconds with good results. Longer acquisitions (e.g., > 15 seconds) are not recommended because it becomes harder to identify early enhancement. The rapidity with which MRI must be acquired necessitates that larger voxels (i.e., lower matrix sizes) must be obtained to maintain adequate signal-to-noise ratios. Thus, DCE-MRI is often not as high in resolution as conventional T2-weighted sequences.

Spatial resolution and temporal resolution need to be adjusted to avoid significant partial volume averaging while obtaining an adequate

sampling of the contrast enhancement over time for each tissue voxel. A summary of vendor-specific parameters used at the authors' institutions is provided in Table 1. Although there is ongoing debate on the imaging parameters needed for optimal spatial and temporal resolution to yield the highest diagnostic performance for DCE-MRI of the prostate, the recently published recommendations from a European consensus meeting suggest optimal temporal resolution of 5 seconds, with maximum temporal resolution of 15 seconds [12]. Depending on the scanner, the number of dynamic series should be as high as possible (typically over a period of approximately 5 minutes) to allow optimal curve fitting.

Dynamic Contrast-Enhanced MRI and Analysis Methods

The analysis of DCE-MRI can be considered in the framework of complexity versus standardization. The most readily accessible analytic method, but also the least standardized, is the qualitative approach. The most complex, but perhaps the most generalizable, method is the quantitative approach. In between is the semiquantitative or "curveology" approach. Next, we will consider each approach.

Qualitative—The qualitative, or visual, analysis of DCE-MRI and its use for prostate imaging is based on the general assumption that tumor vessels are leaky and more readily enhance after IV contrast material is expressed by a fast exchange of blood and contrast media between capillaries and tumor tissues [7]. Thus, DCE-MRI patterns for malignant tumors are expected to show early rapid high enhancement after injection followed by a relatively rapid decline compared with a slower and continuously increasing signal for normal tissues during the first few minutes after contrast injection. Using early (arterial phase) enhancement and morphologic criteria, higher accuracy and less interobserver variability have been reported for DCE-MRI than for T2-weighted MRI. However, there is overlap of malignant and benign tissues, which also varies in different prostate zones, limiting the capabilities of the qualitative DCE-MRI approach. Moreover, the qualitative approach is inherently subjective and therefore difficult to standardize among institutions, making multicenter trials less reliable.

Semiquantitative—The semiquantitative approach is also based on the assumption of early and intense enhancement and washout as a predictor of malignancy. Unlike the visual approach, the semiquantitative analysis

calculates various curve parameters, sometimes collectively referred to as "curveology." Parameters are obtained to characterize the shape of the time-intensity curve, such as the time of first contrast uptake, time to peak, maximum slope, peak enhancement, and wash-in and washout curve shapes. In prostate cancer, there is early intense enhancement and rapid washout of contrast material [3, 13–20] (Fig. 1A).

There are three common dynamic curve types after initial uptake: type 1, persistent increase; type 2, plateau; and type 3, decline

after initial upslope. Type 3 is considered the most suspicious for prostate cancer, especially if there is a focal asymmetric enhancing lesion; however, type 1 and 2 curves can be found in prostate cancer as well (Fig. 1B). Although the semiquantitative approach is widely used in the assessment of DCE-MRI, it has limitations in terms of generalization across acquisition protocols, sequences, and all other factors contributing to the MR signal intensity, which in turn affect curve metrics, such as maximum enhancement and washout percentage.
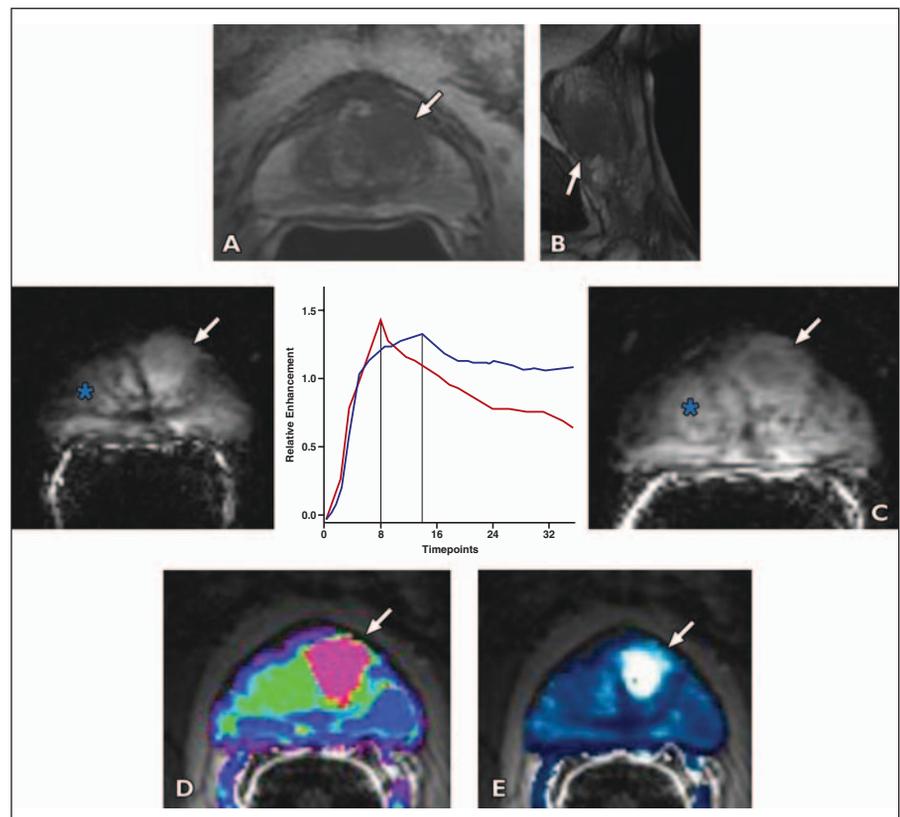

Fig. 3—52-year-old man with prostate cancer of central gland, Gleason score 7 (4 + 3) and prostate-specific antigen level of 19.3 ng/mL who underwent negative transrectal ultrasound prostate biopsy. Endorectal MRI was performed at 3 T for tumor detection. Axial diffusion-weighted image was markedly distorted and nondiagnostic because patient had bilateral hip replacements.
A, Axial T2-weighted image shows ill-defined homogeneous low-signal-intensity masslike region in left central gland (*arrow*).
B, Sagittal T2-weighted image shows homogeneous low-signal-intensity mass far anteriorly in central gland (*arrow*).
C, Early contrast-enhanced T1-weighted gradient-recalled echo image (at peak enhancement) (*right*) shows avid enhancement in left central gland corresponding to T2-weighted abnormality (*arrow*). Benign prostate hypertrophy (BPH) (*asterisk*) is seen in right central gland. Kinetic curve (percentage of enhancement over time) comparison (*center*) is made between prostate cancer (*red*) and BPH (*blue*). Vertical lines show location of peak enhancement. BPH shows longer time to peak when compared with prostate cancer. Late enhancement pattern in BPH in this case shows washout, although to lesser degree than in prostate cancer. This example shows that BPH enhancement curves have characteristics that may closely resemble cancerous tissue. Slightly delayed contrast-enhanced T1-weighted gradient-recalled echo image (just past peak enhancement) (*left*) shows avid enhancement in entire central gland masking tumor (*arrow*) (5.8 s/timpoint).
D and **E,** Fusion of transverse T2-weighted images with color-encoded maps show utility of color map in identifying tumor. K^{trans} (forward volume transfer constant) (**D**) and k_{ep} (reverse reflux rate constant) (**E**) maps delineate tumor area (*arrow*). Pharmacokinetic parameters may be helpful for better differentiation.

Differences in temporal resolution and injection rates can easily change the shape of wash-in/washout curves, making comparison and quantitation difficult. Moreover, these descriptive parameters provide no physiologic insight into the behavior of the tumor vessels. High interpatient variability also hampers the ability to define threshold values for each parameter that could standardize this approach. Nevertheless, the relative simplicity of this approach is appealing, and it has been applied successfully [15]. Thus, relatively simple descriptive parameters are useful in differentiating malignant from normal and pathologic but benign prostatic tissue [3, 21, 22].

Quantitative—During the past decade, the quantitative analysis of DCE-MRI has gained increasing application in prostate imaging because of more widely available software methods and a growing consensus on this approach. The quantitative approach is based on modeling the concentration change of the contrast agent using pharmacokinetic modeling techniques. After the work of Kety [23], which described the flow-limited tracer uptake in tissue, several pharmacokinetic models were proposed by Tofts et al. [24], Brix et al. [25], and Larsson et al. [26]. Most of these models are based on determining the rate of contrast exchange between plasma and extracellular space using transfer rate constants, such as K^{trans} (forward volume transfer constant) and k_{ep} (reverse reflux rate constant between extracellular space and plasma). These constants are known to be elevated in many cancers [27, 28]. The transfer constant, K^{trans}, is equal to the permeability surface area product per unit volume of tissue. K^{trans} determines the flux from the intravascular space to the extracellular space; it may predominantly represent the vascular permeability in a permeability-limited situation (high flow relative to permeability), or it may represent the blood flow into the tissue in a flow-limited situation (high permeability relative to flow) [29]. The v_e is the extracellular extravascular volume fraction, and $k_{ep} = K^{trans} / v_e$ expresses the rate constant, describing the efflux of contrast media from the extracellular space back to plasma. The v_p is the fraction of plasma per unit volume of tissue.

The initial model, described by Tofts et al. [24], developed for blood-brain barrier (BBB) permeability measurements ignored the contribution of the plasma to total tissue concentration, which is acceptable

for normal brain tissues with an intact BBB. However, as the model gained popularity in tumor applications throughout the body, the vascular contribution to signal intensity was included as an extension to this model. In quantitative DCE-MRI analysis, "tissue" is modeled as four compartments: plasma, extracellular space, intracellular space, and kidney excretory pathway. The intracellular space is disregarded in many models because it is assumed that there is no contrast media exchange with the intracellular space, although others have pointed out that water

itself can exchange between the cell and the extracellular space, thereby influencing signal changes in the extracellular space. The pharmacokinetic model (Fig. 1C) is applied to the time-dependent concentration changes of the contrast agent in the artery supplying the tissue of interest, which is the arterial input function (AIF), and the tissue contrast agent concentration [29]. As noted, commercial software packages are now available to input DCE-MRI data and produce parametric maps, such as K^{trans} and k_{ep} maps, that can be used for diagnostic purposes.
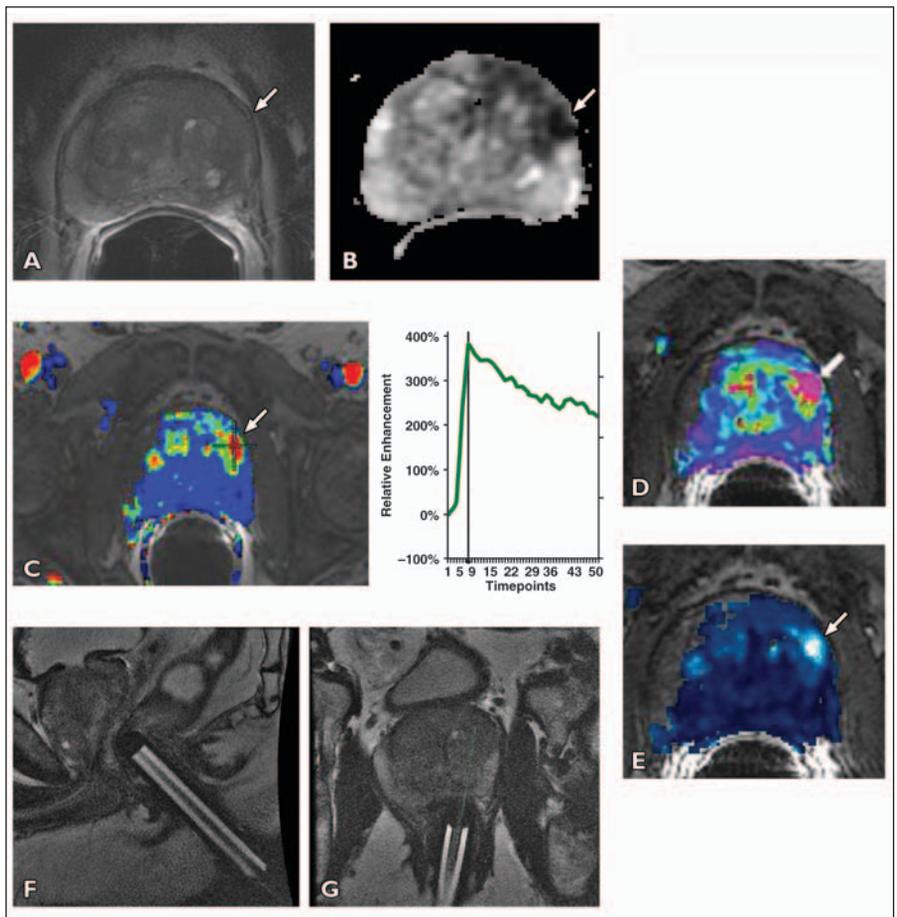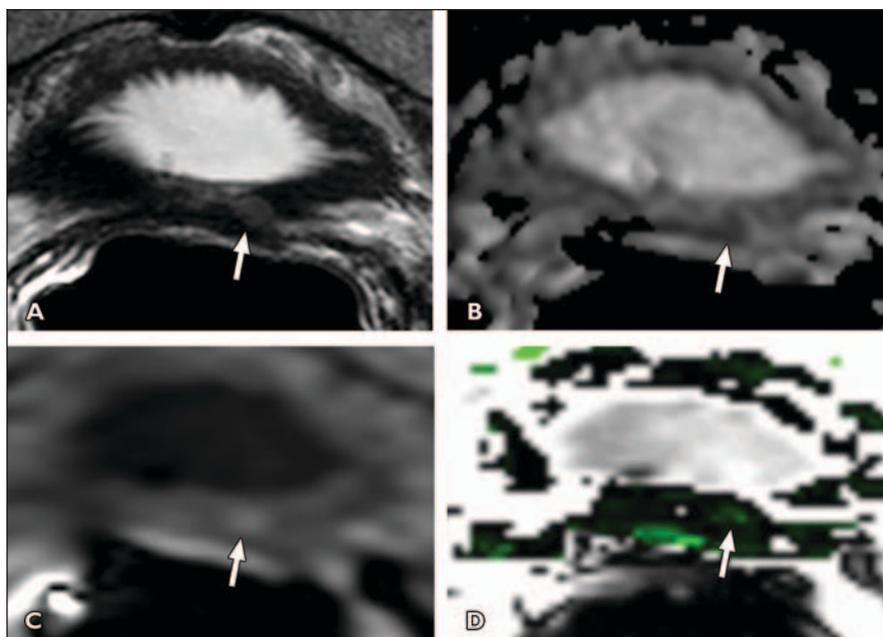

Fig. 4—65-year-old man with prostate-specific antigen level of 29.1 ng/mL and three prior negative transrectal ultrasound–guided prostate biopsies over past 3 years.
A, Axial T2-weighted image shows subtle asymmetric low-signal focus (*arrow*) in left anterior-lateral horn of peripheral zone of midgland.
B, Apparent diffusion coefficient map shows restricted diffusion in left midgland (*arrow*).
C, Contrast-enhanced images are overlaid on T2-weighted MR images (wash-in and washout). Color map shows marked enhancement in left midgland peripheral zone mass (*arrow*). Plot of relative contrast enhancement in regions of interest over time shows earlier onset time, shorter time to peak, high peak enhancement, and early washout of contrast after maximum enhancement in left midgland peripheral zone lesion (5.8 s/timepoint).
D and **E,** Pharmacokinetic parameter maps for K^{trans} (forward volume transfer constant) (**D**) and k_{ep} (reverse reflux rate constant) (**E**) show area of increased exchange constants in left anterior-lateral horn of peripheral zone of midgland (*arrow*).
F and **G,** On basis of MRI results, MRI-guided biopsy was performed by placing endorectal needle guide (**F**). An 18-gauge MRI-compatible needle was introduced through needle guide and two core biopsies were obtained (**G**). Pathology of specimen yielded prostate cancer Gleason score of 7 (4 + 3).

Fig. 5—Local tumor recurrence after prostatectomy seen on multiparametric MRI in 64-year-old man with rising prostate-specific antigen (1.22 ng/dL) 3 months after radical prostatectomy.
A, Axial T2-weighted MR image through resection bed shows minimal soft tissue on left (*arrow*).
B, Axial apparent diffusion coefficient image shows signal restriction suggesting tumoral pattern (*arrow*).
C, Axial raw dynamic contrast-enhanced MR image shows early and diffuse enhancement within left-sided nodular lesion (*arrow*).
D, Reverse reflux rate constant (k_{ep}) map derived from dynamic contrast-enhanced MR image also localizes left-sided area of nodular enhancement, compatible with local recurrence (*arrow*).

It is important to remember that signal intensity must be converted to T1 values on the basis of a T1 map because MRI signal intensity is not linear with the gadolinium concentration and the pharmacokinetic models require concentration values. Thus, T1 maps are used to generate the concentration curves of the contrast agent. Moreover, some models also use AIF, which is individualized to each patient or pooled on the basis of populations of patients. Fortunately, a number of software programs can now produce parametric color maps using these model-based parameters and can be overlaid on T2-weighted images. These maps can be computed after correcting for signal intensity and motion (Fig. 2).

Even though a more complex approach than semiquantitative methods, quantitative modeling has the potential for standardization across various sequences and parameters. DCE-MRI–driven physiologic parameters, such as K^{trans} and k_{ep}, are elevated in prostate cancer and have been used to detect malignancy in the prostate, often in a multiparametric approach in combination with other sequences: T2-weighted MRI, DWI, and MRSI [30–32]. Obtaining stable measurements from quantitative methods remains a challenge because of the number of variables that can affect it, including changes in cardiac output, challenges in measuring tissue T1, and problems with measurement of a tissue AIF. In addition, angiogenesis is not a constant feature of all tumors, especially small ones, and not all angiogenesis is due

to cancer but can also be caused by inflammatory conditions. Because of considerable overlap of the rate constants for benign and cancerous tissue, DCE-MRI, whether qualitative or quantitative, must always be read in conjunction with T2-weighted images and DWI or MRSI to obtain better diagnostic performance [33–38]. Given the complexi-
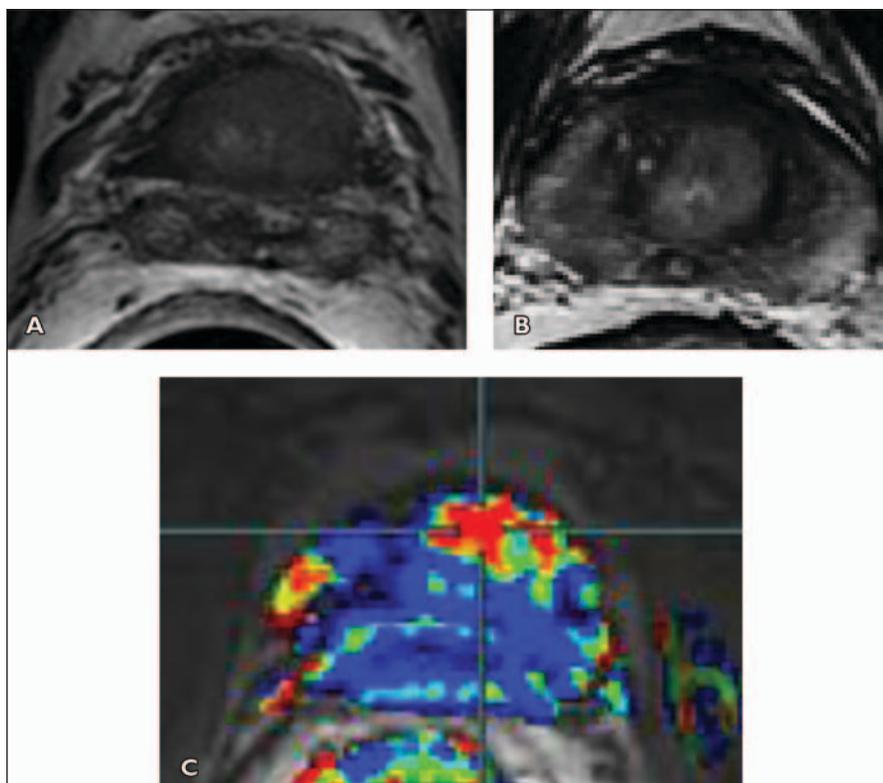
ty and limitations of a fully quantitative acquisition and analysis, visual and semiquantitative methods are often substituted when quantitation is less important.

Image Interpretation

Consensus guidelines are being developed internationally for the interpretation of pros-

Fig. 6—Local tumor recurrence in 57-year-old man who underwent electron-beam radiotherapy because of tumor with Gleason score of 7 (3 + 4) in left base 3 years ago. Prostate-specific antigen was 2.15 ng/dL at time of multiparametric MRI.
A and **B,** Axial T2-weighted images show diffuse low signal throughout base with no definite tumor.
C, Contrast-enhanced images are overlaid on T2-weighted MR image. Wash-in and washout color map shows marked enhancement in anterior base (*cross-hair*).
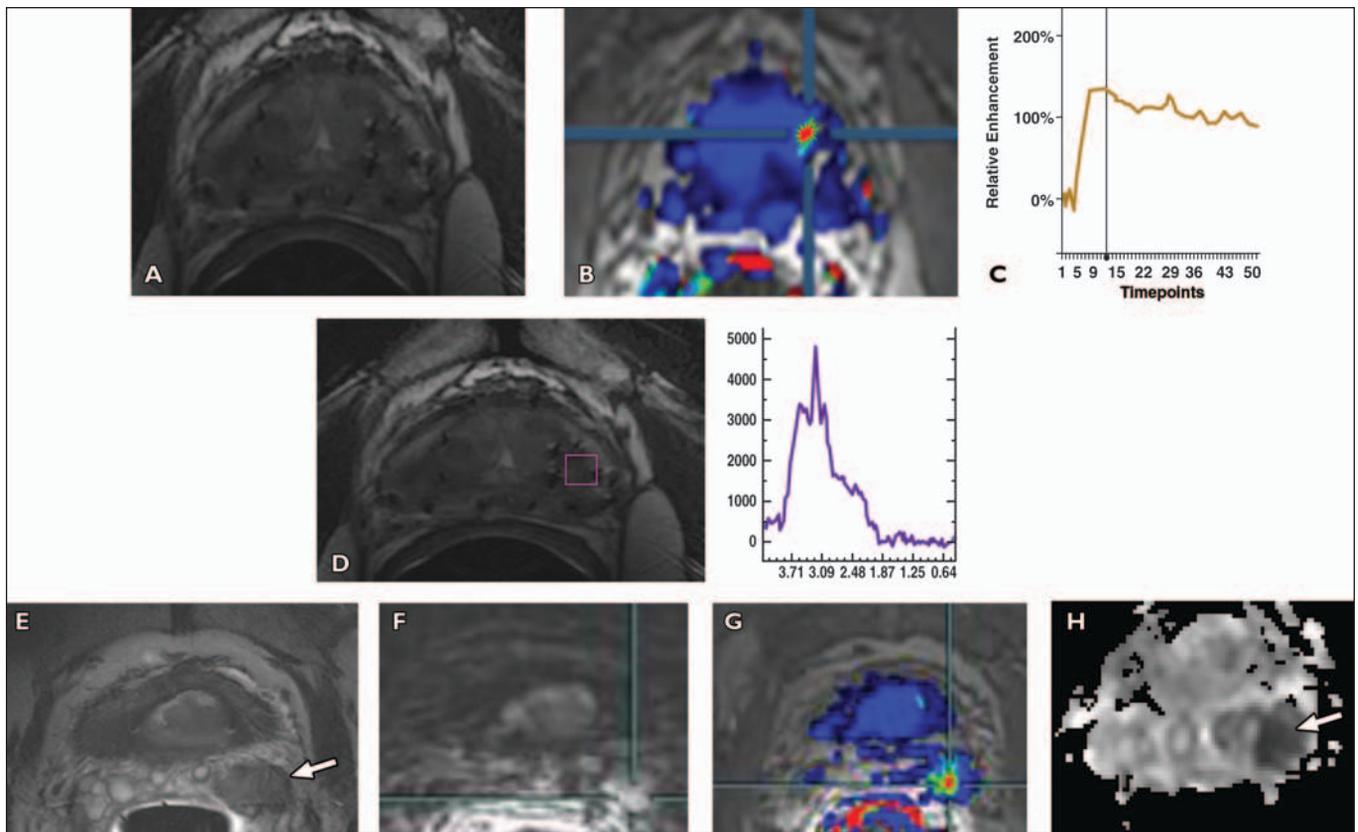
Fig. 7—Local tumor recurrence after brachytherapy in 67-year-old man with Gleason score of 7 (3 + 4) in left midgland who underwent transperineal radioactive ^{125}I seed implantation 8 years ago. Patient had slowly rising prostate-specific antigen level over several years, with level of 2.9 ng/dL at time of multiparametric MRI.

A, Axial T2-weighted image shows featureless prostate gland with ^{125}I seeds and no definite tumor. Diffusion-weighted image showed no signal restriction within prostate gland.

B, Contrast-enhanced images are overlaid on T2-weighted MRI. Wash-in and washout color map shows marked enhancement in left midgland peripheral zone (*cross-hair*).

C, Plot of relative contrast enhancement in regions of interest over time shows earlier onset time, shorter time to peak, high peak enhancement, and early washout of contrast material in left midgland peripheral zone lesion (5.8 s/timepoint).

D, MR spectroscopy image overlying axial T2-weighted image (*purple voxel*) in left midgland shows metabolites at 3.2 ppm, corresponding to high (cho) peak and atrophy in remainder of gland.

E, Axial T2-weighted image shows asymmetric low-signal-intensity enlargement of seminal vesicle on left (*arrow*).

F and **G,** Axial raw dynamic contrast-enhanced MR image (**F**) and color map (**G**) show early intense enhancement in left seminal vesicle lesion (*cross-hair*).

H, Apparent diffusion coefficient map derived from diffusion-weighted image shows focal signal restriction in seminal vesicle (*arrow*). This feature is diagnostic of tumor recurrence.

tate MRI [39]; however, there is general agreement on the major components of multiparametric MRI. The peripheral zone is typically interpreted distinctly from the central gland. T2-weighted imaging is the oldest and most studied of the MR sequences. Prostate cancer is characterized by low T2 signal intensity replacing the normally high T2 signal intensity in the peripheral zone (Fig. 2A). However, focal decreases in T2 signal intensity can be caused by benign processes, and many cancers show minimally reduced T2 signal, making them nearly isointense on T2-weighted images. DWI has become a more important ancillary sequence in prostate MRI because of improvements in the ability to suppress susceptibility artifacts. Tumors show re-

duced diffusion, resulting in higher signal on images with a high b value and reduced signal on apparent diffusion coefficient (ADC) maps. ADC values correlate with the Gleason score of prostate cancers [40–42]. DCE-MRI is commonly used in conjunction with at least two other MR sequences. For instance, regions of the prostate that are low in T2 signal but that also show rapid wash-in and washout or high K^{trans} or k_{ep} are more suspicious for cancer. Thus, these sequences are used together and are highly dependent on each other.

Prostate cancer arising in the central gland (transition zone, central zone, and anterior fibromuscular stroma) are more difficult to diagnose because of the heterogeneity of signal intensity arising from benign prostatic hyper-

plasia (BPH). On T2-weighted images, the diagnosis of a central gland tumor [43] is supported by findings of homogeneous low T2 signal intensity, ill-defined irregular edges of the suspicious lesion, invasion into the urethra or the anterior fibromuscular stroma, lack of the low-signal-intensity rim commonly seen in association with BPH, and lenticular shape [44] (Fig. 3).

However, these findings can be misleading because low signal intensity can also be seen in the stromal type of BPH. Thus, in many studies, the performance of MRI for the localization of central gland tumors is either not specifically reported or lower than for peripheral gland tumors [45]. A growing number of MRI studies have shown that the detection
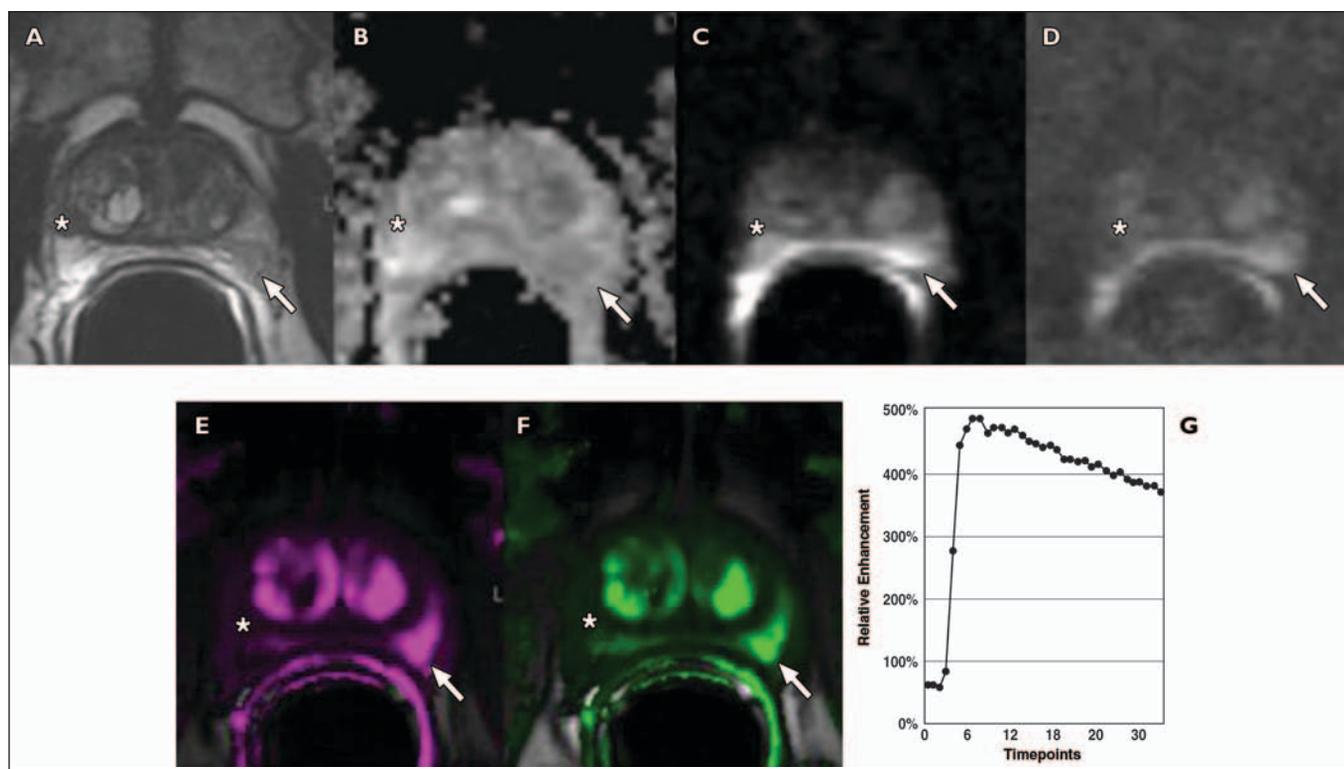
Fig. 8—Focal prostatitis simulating prostate cancer in 64-year-old man with rising prostate-specific antigen (PSA) level at two PSA levels (5, and 7 ng/m,) with normal digital rectal examination. Asterisks indicate benign appearance of contralateral nodule showing no restriction of diffusion and no vascularity. Directed biopsies in both nodules as well as sextant biopsies were negative. PSA level returned to baseline 3 months after biopsy.

A, T2-weighted image shows hypointense signal in left peripheral zone (*arrow*).

B–D, Apparent diffusion coefficient map derived from diffusion-weighted image (**B**) shows moderate signal restriction and bright focal signal of left peripheral zone (*arrow*), which is more conspicuous at b2000 value (**D**) than at b1000 value (**C**).

E–G, Color maps, K^{trans} (forward volume transfer constant) (**E**) and k_{ep} (reverse reflux rate constant) (**F**), and semiquantitative analysis (**G**) show high color-coded values of dynamic parameters, K^{trans} and k_{ep} (*arrow*), and type 3 curve at semiquantitative analysis (8.5 s/timepoint).

and characterization of prostate cancer can be significantly improved by performing the imaging examination on higher magnetic field strength MR scanners (3 T) and using either DWI or MRSI with DCE-MRI [34–37, 46]. In a multiparametric MRI examination, the high sensitivity of DCE-MRI may be used to select lesions for biopsy. Thus, DCE-MRI is interpreted both independently and together with other sequences (Fig. 4).

Clinical Experience With Dynamic Contrast-Enhanced MRI
Diagnosis and Local Staging

The performance of DCE-MRI is usually reported for tumors of significant volume (> 0.5 mL) and Gleason grade (≥ 6) [47]. DCE-MRI alone has reported sensitivity and specificity ranges of 46–96% and 74–96%, respectively, for detection of tumors, but, as always, these ranges are highly dependent on patient selection, technique and diagnostic criteria at MRI, pathology correlation method (biopsy vs whole mount), and tumor size [48–55].

A study of DCE-MRI and combined DCE-MRI-MRSI in 150 patients with a negative prior transrectal ultrasound–guided prostate biopsy showed that DCE-MRI had sensitivity, specificity, and positive and negative predictive values of 76.5%, 89.5%, 84.5%, and 83.7%, respectively, and these numbers improved with the combined use of DCE-MRI and MRSI [46]. Others have shown a high correlation of DCE-MRI findings in prostate cancer with whole-mount histopathology [48, 51, 55]. Thus, DCE-MRI contributes valuable information to prostate MRI.

In the last decade, the multiparametric approach has been shown to improve the accuracy of prostate MRI. Thus, DCE-MRI must always be viewed in the context of other MRI parameters. For instance, one study showed that combining T2-weighted MRI with DWI and DCE-MRI led to sensitivity of 83%, whereas the sensitivity of DCE-MRI alone was only 43% [36]. Recently, Turkbey et al. [37] reported that a four-sequence multiparametric approach (T2-weighted, DWI, DCE-MRI, and

MRSI) had sensitivity of 86% and specificity of nearly 100% in a prospective trial of 45 patients. Multiparametric MRI has been more successful in the peripheral zone than the central gland [35]. A recent study reported that combined use of ADC maps and K^{trans} values extracted from DCE-MRI improved tumor detection in the central gland [38]. As experience grows and technology improves, the multiparametric MRI approach has also improved and very acceptable detection rates can now be obtained from both the peripheral zone and central gland.

Detection of Tumor Recurrence:
PSA Relapse After Treatment

Patients are followed by serum PSA and digital rectal examination after treatment of prostate cancer. Currently, clinical nomograms are used to predict the risk of biochemical recurrence; however, these nomograms have some limitations related to their variables, such as the low specificity of serum PSA and underestimated Gleason score at biopsy.
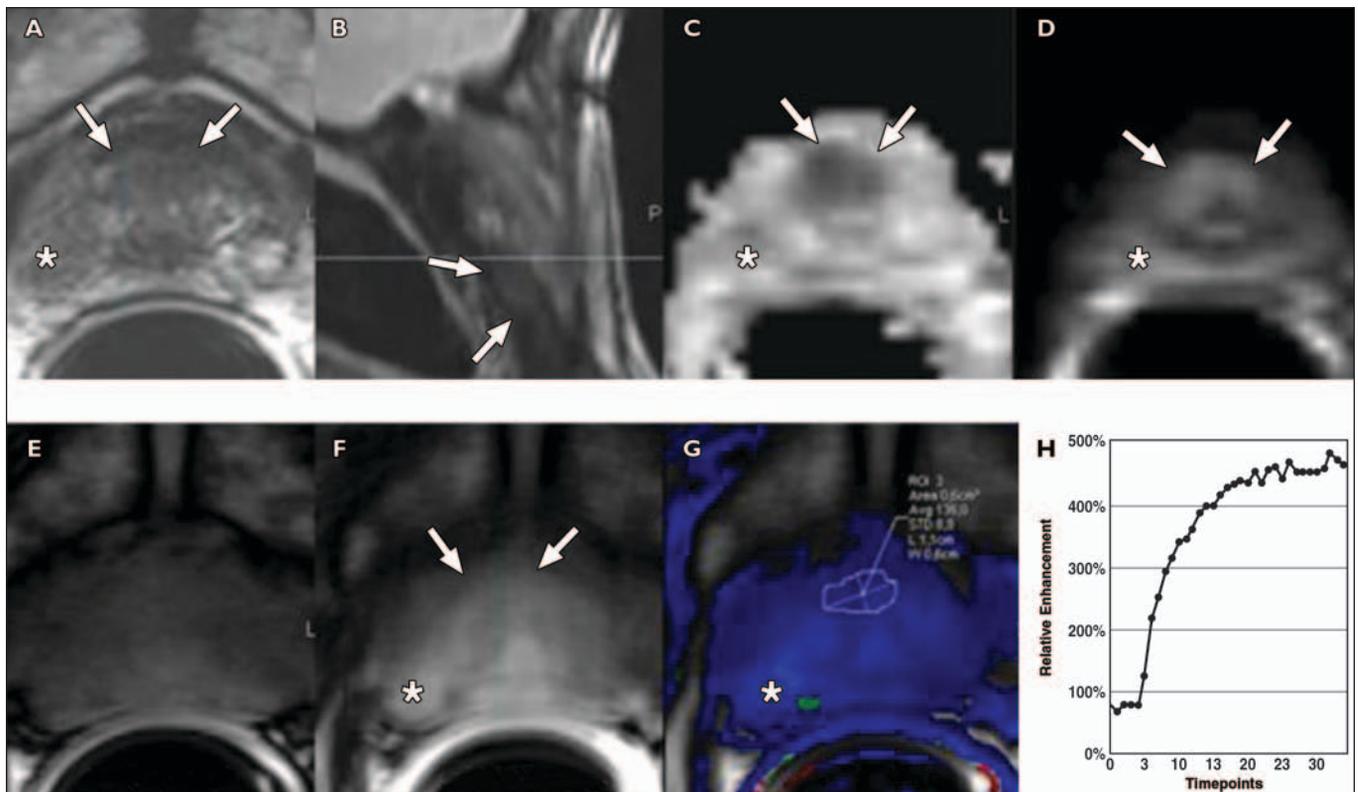
Fig. 9—Anterior hypovascular central gland carcinoma in 68-year-old man with prostate-specific antigen level of 11 ng/mL. One set of 12 transrectal ultrasound (TRUS)-guided prostate biopsy results was negative. Images show focal right nonspecific hypointense signal (*asterisk*, **A**) with no significant restriction of diffusion (*asterisk*, **C** and **D**), and no washout on color-coded quantitative dynamic contrast-enhanced (DCE) map (*asterisk*, **F** and **G**). Four of four positive anterior biopsies directed within anterior hypointense signal yielded prostate adenocarcinoma, Gleason score of 6, cancer length of 24 mm, negative biopsies in right peripheral zone and in 12 TRUS-guided prostate biopsies.
A and **B**, Axial (**A**) and sagittal (**B**) T2-weighted MR images show anterior apical homogeneous ill-defined lenticular hypointense signal (*arrows*), suggesting central gland tumor.
C and **D**, Low apparent diffusion coefficient value (**C**) and bright signal intensity at b1000 diffusion-weighted (**D**) images suggest malignancy (*arrows*).
E and **F**, Unenhanced (**E**) and qualitative DCE (**F**) MR images show no significant enhancement in anterior focal area (*arrows*, **F**).
G and **H**, Low-color-coded k_{ep} (reverse reflux rate constant) value (**G**) and type 1 semiquantitative DCE curve (8.5 s/timepoint) (**H**) suggest benign tissue.

DCE-MRI has shown the ability to detect cancer recurrence when PSA begins to rise after a nadir in patients who have undergone radical prostatectomy (Fig. 5). For instance, biochemical relapse after radical prostatectomy can occur in 15–30% of patients [56–59]. Detection of tumor recurrence after radical treatment can be difficult because the lack of normal landmarks and the presence of scar tissue can lead to uncertainty. Determining the site of recurrence is important because patients with isolated local recurrence can benefit from further treatments, such as radiation to the prostatectomy resection bed.

Panebianco et al. [60] evaluated 84 patients with suspected local recurrence after prostatectomy using conventional MRI with MR spectroscopy and DCE-MRI as well as ^{18}F-choline PET/CT and concluded that accuracy was greater for multiparametric MRI than for PET/CT (area under the curve of MRI and PET/CT, 0.971 and 0.837, respectively).

Biochemical recurrence can occur in 20–40% of patients who undergo external-beam radiation therapy (EBRT) [61]. Detecting recurrence after radiation therapy can be clinically challenging because the PSA level may not be a reliable marker, and the digital rectal examination can be nonspecific due to fibrotic changes in the irradiated prostate gland. Multiparametric MRI, specifically DCE-MRI and MRSI, have shown the ability to identify tumor recurrence (Figs. 6 and 7) with high accuracy in postradiotherapy patients [62–64].

Naturally, the most likely site for residual disease after radiation therapy is the site of the original primary tumor [65], supporting the practice of boosting the radiation dose to the primary tumor. For prediction of local tumor progression of prostate cancer after high-intensity focused ultrasound ablation, DCE-MRI was more sensitive than T2-weighted MRI with DWI [66]. These results suggest

that patients who have a rising PSA level after therapy may benefit from an MRI examination to detect recurrent or residual disease.

Limitation and Pitfalls

Despite its advantages, there are a number of limitations to DCE-MRI. A major source of error in DCE-MRI is motion. Motion arises from rectal peristalsis and bladder filling as well as bulk patient movement. Because the DCE-MRI study extends over 5 or more minutes, significant misregistration between consecutive slices can occur. This can lead to noise in the wash-in and wash-out curves, leading to difficulty in fitting the curve with pharmacokinetic models. For instance, marked anterior prostatic displacements due to rectal motion can occur during DCE-MRI examinations and can lead to noisy curves [3, 67]. Commercially available DCE-MRI postprocessing software has been introduced to correct for motion by automat-
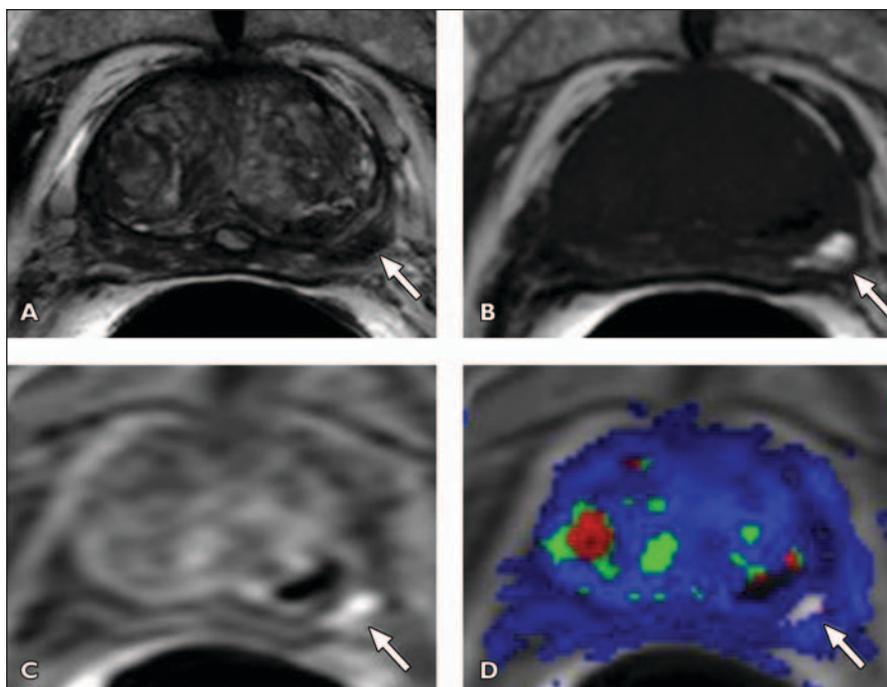
Fig. 10—Hemorrhage masking prostate cancer in left midgland in 77-year-old man with serum prostate-specific antigen level of 1.7 ng/dL. Biopsy was performed 8 weeks prior to MRI.
A, Axial T2-weighted MR image shows left midgland peripheral zone lesion (*arrow*).
B, Axial T1-weighted MR image shows biopsy related residual hemorrhage within lesion (*arrow*).
C, Axial raw dynamic contrast-enhanced (DCE) MR image shows no enhancement within left midgland peripheral zone lesion secondary to presence of hemorrhage (*arrow*).
D, K^{trans} (forward volume transfer constant) map derived from DCE MR image is also affected by presence of hemorrhage (*arrow*). Pathologic correlation after prostatectomy yielded prostate adenocarcinoma, with Gleason score of 6 in left midgland.

ically repositioning the sequential images so they align better with each other.

A central limitation of DCE-MRI is that it is nonspecific. Increased vessel leakiness can be seen in prostatitis in the peripheral zone (Fig. 8) and in highly vascularized BPH nodules in the central gland. Additionally, anterior hypovascular transitional zone tumors may not show DCE-MRI uptake (Fig. 9). Residual postbiopsy hemorrhage can also lead to both false-negative (Fig. 10) and false-positive results. Thus, DCE-MRI must always be viewed in the context of other MRI parameters and cannot stand alone as a diagnostic modality regardless of curve shape or intensity of enhancement.

Because investigators use different DCE-MRI sequences and different methods of analysis, there is a lack of standardization in the performance of DCE-MRI, making it difficult to compare published studies. Shorter acquisition times (< 5 seconds per 3D acquisition) have generally proven to be more valuable in prostate cancer than longer acquisition times, but one cannot reasonably compare two studies performed with markedly different acquisition times. Moreover, the use of AIFs, individualized or pooled, is another source of variability among studies. Because there has been an increase in availability of commercially available postprocessing tools, it is important to pay attention to how these available tools process the DCE-MRI data to generate parametric maps. Differences in postprocessing algorithms can also account for observed differences in the metrics of tumor vascularity. To enable further investigation of the value of DCE-MRI of the prostate, the technique of DCE-MRI and the pharmacokinetic model used to analyze it must become more standardized.

Future Directions

The role of DCE-MRI in prostate cancer detection is not in dispute. Looking forward, a major area of development is international standards so that the technique can be tested in multicenter trials. Because of its complexity, DCE-MRI may also benefit from automated decision-support systems that suggest to the radiologist areas of abnormality on MRI. These have been successfully applied in screening mammography and breast MRI.

They may prove even more useful in the prostate, where the complexity of image interpretation poses even more burdens on the generalist. Also anticipated are further improvements in technology that will enable faster 3D acquisitions with built-in motion compensation to improve the quality of the curves generated from DCE-MRI.

Conclusion

DCE-MRI techniques are becoming more widely available in clinical practice. The analysis of this dynamic data can be performed with simple visual or semiquantitative approaches or more complex nonstandardized quantitative approaches using pharmacokinetic models. DCE-MRI and the corresponding pharmacokinetic models and parameters have shown great potential for improving the diagnosis of prostate cancer by adding functional information to the anatomic information provided by conventional MRI sequences. Semiquantitative methods may be sufficient for the principal clinical needs of prostate cancer localization and staging. Further clinical validation is necessary to justify the need for a fully quantitative approach to DCE-MRI in prostate cancer localization and staging in current clinical practice.

Initial clinical applications of DCE-MRI, including the detection, localization, and staging of prostate cancer as well as the diagnosis of recurrence, show that the technique offers diagnostic benefits when compared with conventional MRI alone and as part of a multiparametric prostate MRI examination. For the radiologist embarking on the use of these techniques, it is essential to develop an understanding of the need for rapid acquisition, overlap with other diseases (prostatitis, BPH), and familiarity with a variety of analytic methods. Understanding the relative advantages, limitations, and potential pitfalls will improve the interpretation of DCE-MRI results.

References

1. Jemal A, Siegel R, Ward E, Hao Y, Xu J, Thun MJ. Cancer statistics, 2009. *CA Cancer J Clin* 2009; 59:225–249

2. Thompson IM, Pauler DK, Goodman PJ, et al. Prevalence of prostate cancer among men with a prostate-specific antigen level ≤ 4.0 ng per milliliter. *N Engl J Med* 2004; 350:2239–2246 [erratum in *N Engl J Med* 2004; 351:1470]

3. Engelbrecht MR, Huisman HJ, Laheij RJ, et al. Discrimination of prostate cancer from normal peripheral zone and central gland tissue by using dynamic contrast-enhanced MR imaging. *Radiology* 2003; 229:248–254

4. Nicholson B, Schaefer G, Theodorescu D. Angiogenesis in prostate cancer: biology and therapeutic opportunities. *Cancer Metastasis Rev* 2001; 20:297–319

5. Bigler SA, Deering RE, Brawer MK. Comparison of microscopic vascularity in benign and malignant prostate tissue. *Hum Pathol* 1993; 24:220–226

6. Siegal JA, Yu E, Brawer MK. Topography of neovascularity in human prostate carcinoma. *Cancer* 1995; 75:2545–2551

7. Erbersdobler A, Isbarn H, Dix K, et al. Prognostic value of microvessel density in prostate cancer: a tissue microarray study. *World J Urol* 2010; 28:687–692

8. Mucci LA, Powolny A, Giovannucci E, et al. Prospective study of prostate tumor angiogenesis and cancer-specific mortality in the Health Professionals Follow-Up Study. *J Clin Oncol* 2009; 27:5627–5633

9. Brawer MK, Deering RE, Brown M, Preston SD, Bigler SA. Predictors of pathologic stage in prostatic carcinoma: the role of neovascularity. *Cancer* 1994; 73:678–687

10. Barentsz JO, Jager G, Mugler JP 3rd, et al. Staging urinary bladder cancer: value of T1-weighted three-dimensional magnetization prepared-rapid gradient-echo and two-dimensional spin-echo sequences. *AJR* 1995; 164:109–115

11. Boetes C, Barentsz JO, Mus RD, et al. MR characterization of suspicious breast lesions with a gadolinium-enhanced turboFLASH subtraction technique. *Radiology* 1994; 193:777–781

12. Dickinson L, Ahmed HU, Allen C, et al. Magnetic resonance imaging for the detection, localisation, and characterisation of prostate cancer: recommendations from a European consensus meeting. *Eur Urol* 2011; 59:477–494

13. Fütterer JJ, Engelbrecht MR, Huisman HJ, et al. Staging prostate cancer with dynamic contrast-enhanced endorectal MR imaging prior to radical prostatectomy: experienced versus less experienced readers. *Radiology* 2005; 237:541–549

14. Haider MA, Chung P, Sweet J, et al. Dynamic contrast-enhanced magnetic resonance imaging for localization of recurrent prostate cancer after external beam radiotherapy. *Int J Radiat Oncol Biol Phys* 2008; 70:425–430

15. Noworolski SM, Henry RG, Vigneron DB, Kurhanewicz J. Dynamic contrast-enhanced MRI in normal and abnormal prostate tissues as defined by biopsy, MRI, and 3D MRSI. *Magn Reson Med* 2005; 53:249–255

16. Puech P, Betrouni N, Makni N, Dewalle AS, Villers A, Lemaitre L. Computer-assisted diagnosis of prostate cancer using DCE-MRI data: design, implementation and preliminary results. *Int J Comput Assist Radio Surg* 2009; 4:1–10

17. Somford DM, Fütterer JJ, Hambrock T, Barentsz JO. Diffusion and perfusion MR imaging of the prostate. *Magn Reson Imaging Clin N Am* 2008; 16:685–695

18. Casciani E, Polettini E, Carmenini E, et al. Endorectal and dynamic contrast-enhanced MRI for detection of local recurrence after radical prostatectomy. *AJR* 2008; 190:1187–1192

19. Bloch BN, Furman-Haran E, Helbich TH, et al. Prostate cancer: accurate determination of extracapsular extension with high-spatial-resolution dynamic contrast-enhanced and T2-weighted MR imaging—initial results. *Radiology* 2007; 245:176–185

20. Carlani M, Mancino S, Bonanno E, Finazzi Agro E, Simonetti G. Combined morphological, [^{1}H]-MR spectroscopic and contrast-enhanced imaging of human prostate cancer with a 3-Tesla scanner: preliminary experience. *Radiol Med (Torino)* 2008; 113:670–688

21. Jackson AS, Reinsberg SA, Sohaib SA, et al. Dynamic contrast-enhanced MRI for prostate cancer localization. *Br J Radiol* 2009; 82:148–156

22. Kiessling F, Lichy M, Grobholz R, et al. Simple models improve the discrimination of prostate cancers from the peripheral gland by T1-weighted dynamic MRI. *Eur Radiol* 2004; 14:1793–1801

23. Kety SS. The theory and applications of the exchange of inert gas at the lungs and tissues. *Pharmacol Rev* 1951; 3:1–41

24. Tofts PS, Wicks DA, Barker GJ. The MRI measurement of NMR and physiological parameters in tissue to study disease process. *Prog Clin Biol Res* 1991; 363:313–325

25. Brix G, Semmler W, Port R, Schad LR, Layer G, Lorenz WJ. Pharmacokinetic parameters in CNS Gd-DTPA enhanced MR imaging. *J Comput Assist Tomogr* 1991; 15:621–628

26. Larsson HB, Stubgaard M, Frederiksen JL, Jensen M, Henriksen O, Paulson OB. Quantitation of blood-brain barrier defect by magnetic resonance imaging and gadolinium-DTPA in patients with multiple sclerosis and brain tumors. *Magn Reson Med* 1990; 16:117–131

27. van Dorsten FA, van der Graaf M, Engelbrecht MR, et al. Combined quantitative dynamic contrast-enhanced MR imaging and (1)H MR spectroscopic imaging of human prostate cancer. *J Magn Reson Imaging* 2004; 20:279–287

28. Knopp MV, Giesel FL, Marcos H, von Tengg-Kobligk H, Choyke P. Dynamic contrast-enhanced magnetic resonance imaging in oncology. *Top Magn Reson Imaging* 2001; 12:301–308

29. Tofts PS, Brix G, Buckley DL, et al. Estimating kinetic parameters from dynamic contrast-enhanced T(1)-weighted MRI of a diffusable tracer: standardized quantities and symbols. *J Magn Reson Imaging* 1999; 10:223–232

30. Turkbey B, Pinto PA, Mani H, et al. Prostate cancer: value of multiparametric MR imaging at 3 T for detection—histopathologic correlation. *Radiology* 2010; 255:89–99

31. Fütterer JJ, Heijmink SW, Scheenen TW, et al. Prostate cancer localization with dynamic contrast-enhanced MR imaging and proton MR spectroscopic imaging. *Radiology* 2006; 241:449–458

32. Schmuecking M, Boltze C, Geyer H, et al. Dynamic MRI and CAD vs. choline MRS: where is the detection level for a lesion characterisation in prostate cancer? *Int J Radiat Biol* 2009; 85:814–824

33. Panebianco DL, Maes A. Estimating time to steady state using the effective rate of drug accumulation. *Pharm Stat* 2011; 10:27–33

34. Sciarra A, Panebianco V, Ciccariello M, et al. Value of magnetic resonance spectroscopy imaging and dynamic contrast-enhanced imaging for detecting prostate cancer foci in men with prior negative biopsy. *Clin Cancer Res* 2010; 16:1875–1883

35. Scherr MK, Seitz M, Muller-Lisse UG, Ingrisch M, Reiser MF, Muller-Lisse UL. MR-perfusion (MRP) and diffusion-weighted imaging (DWI) in prostate cancer: quantitative and model-based gadobenate dimeglumine MRP parameters in detection of prostate cancer. *Eur J Radiol* 2010; 76:359–366

36. Tamada T, Sone T, Higashi H, et al. Prostate cancer detection in patients with total serum prostate-specific antigen levels of 4–10 ng/mL: diagnostic efficacy of diffusion-weighted imaging, dynamic contrast-enhanced MRI, and T2-weighted imaging. *AJR* 2011; 197:664–670

37. Turkbey B, Mani H, Shah V, et al. Multiparametric 3T prostate magnetic resonance imaging to detect cancer: histopathological correlation using prostatectomy specimens processed in customized magnetic resonance imaging based molds. *J Urol* 2011; 186:1818–1824

38. Oto A, Kayhan A, Jiang Y, et al. Prostate cancer: differentiation of central gland cancer from benign prostatic hyperplasia by using diffusion-weighted and dynamic contrast-enhanced MR imaging. *Radiology* 2010; 257:715–723

39. Barentsz JO, Richenberg J, Clements R, et al. ESUR prostate MR guidelines 2012. *Eur Radiol* 2012; 22:746–757

40. Verma S, Rajesh A, Morales H, et al. Assessment of aggressiveness of prostate cancer: correlation of apparent diffusion coefficient with histologic grade after radical prostatectomy. *AJR* 2011; 196:374–381

41. Turkbey B, Shah VP, Pang Y, et al. Is apparent diffusion coefficient associated with clinical risk scores for prostate cancers that are visible on 3-T MR images? *Radiology* 2011; 258:488–495

42. Hambrock T, Somford DM, Huisman HJ, et al. Relationship between apparent diffusion coefficients at 3.0-T MR imaging and Gleason grade in peripheral zone prostate cancer. *Radiology* 2011;

259:453–461

43. Hricak H, Choyke PL, Eberhardt SC, Leibel SA, Scardino PT. Imaging prostate cancer: a multidisciplinary perspective. *Radiology* 2007; 243:28–53

44. Akin O, Sala E, Moskowitz CS, et al. Transition zone prostate cancers: features, detection, localization, and staging at endorectal MR imaging. *Radiology* 2006; 239:784–792

45. Delongchamps NB, Rouanne M, Flam T, et al. Multiparametric magnetic resonance imaging for the detection and localization of prostate cancer: combination of T2-weighted, dynamic contrast-enhanced and diffusion-weighted imaging. *BJU Int* 2011; 107:1411–1418

46. Panebianco V, Sciarra A, Ciccariello M, et al. Role of magnetic resonance spectroscopic imaging ([(1)H]MRSI) and dynamic contrast-enhanced MRI (DCE-MRI) in identifying prostate cancer foci in patients with negative biopsy and high levels of prostate-specific antigen (PSA). *Radiol Med (Torino)* 2010; 115:1314–1329

47. Oon SF, Watson RW, O'Leary JJ, Fitzpatrick JM. Epstein criteria for insignificant prostate cancer. *BJU Int* 2011; 108:518–525

48. Ocak I, Bernardo M, Metzger G, et al. Dynamic contrast-enhanced MRI of prostate cancer at 3 T: a study of pharmacokinetic parameters. *AJR* 2007; 189:849; [web]W192–W201

49. Tamada T, Sone T, Jo Y, et al. Prostate cancer: relationships between postbiopsy hemorrhage and tumor detectability at MR diagnosis. *Radiology* 2008; 248:531–539

50. Kim JK, Hong SS, Choi YJ, et al. Wash-in rate on the basis of dynamic contrast-enhanced MRI: usefulness for prostate cancer detection and localization. *J Magn Reson Imaging* 2005; 22:639–646

51. Villers A, Puech P, Mouton D, Leroy X, Ballereau C, Lemaitre L. Dynamic contrast enhanced, pelvic phased array magnetic resonance imaging of localized prostate cancer for predicting tumor volume: correlation with radical prostatectomy findings. *J Urol* 2006; 176:2432–2437

52. Cheikh AB, Girouin N, Colombel M, et al. Evaluation of T2-weighted and dynamic contrast-enhanced MRI in localizing prostate cancer before repeat biopsy. *Eur Radiol* 2009; 19:770–778

53. Ogura K, Maekawa S, Okubo K, et al. Dynamic endorectal magnetic resonance imaging for local staging and detection of neurovascular bundle involvement of prostate cancer: correlation with histopathologic results. *Urology* 2001; 57:721–726

54. Lemaitre L, Puech P, Poncelet E, et al. Dynamic contrast-enhanced MRI of anterior prostate cancer: morphometric assessment and correlation with radical prostatectomy findings. *Eur Radiol* 2009; 19:470–480

55. Isebaert S, De Keyzer F, Haustermans K, et al. Evaluation of semi-quantitative dynamic contrast-enhanced MRI parameters for prostate cancer in correlation to whole-mount histopathology. *Eur J Radiol* 2012; 81:e217–e222

56. Han M, Partin AW, Zahurak M, Piantadosi S, Epstein JI, Walsh PC. Biochemical (prostate specific antigen) recurrence probability following radical prostatectomy for clinically localized prostate cancer. *J Urol* 2003; 169:517–523

57. Catalona WJ, Smith DS. 5-year tumor recurrence rates after anatomical radical retropubic prostatectomy for prostate cancer. *J Urol* 1994; 152:1837–1842

58. Kattan MW, Wheeler TM, Scardino PT. Postoperative nomogram for disease recurrence after radical prostatectomy for prostate cancer. *J Clin Oncol* 1999; 17:1499–1507

59. Zincke H, Oesterling JE, Blute ML, Bergstralh EJ, Myers RP, Barrett DM. Long-term (15 years) results after radical prostatectomy for clinically localized (stage T2c or lower) prostate cancer. *J Urol* 1994; 152:1850–1857

60. Panebianco V, Sciarra A, Lisi D, et al. Prostate cancer: 1HMRS-DCEMR at 3T versus [(18)F] choline PET/CT in the detection of local prostate cancer recurrence in men with biochemical progression after radical retropubic prostatectomy (RRP). *Eur J Radiol* [Epub 2011 Feb 15]

61. Kuban DA, Thames HD, Levy LB, et al. Long-term multi-institutional analysis of stage T1-T2 prostate cancer treated with radiotherapy in the PSA era. *Int J Radiat Oncol Biol Phys* 2003; 57:915–928

62. Akin O, Gultekin DH, Vargas HA, et al. Incremental value of diffusion weighted and dynamic contrast enhanced MRI in the detection of locally recurrent prostate cancer after radiation treatment: preliminary results. *Eur Radiol* 2011; 21:1970–1978

63. Kara T, Akata D, Akyol F, Karcaaltincaba M, Ozmen M. The value of dynamic contrast-enhanced MRI in the detection of recurrent prostate cancer after external beam radiotherapy: correlation with transrectal ultrasound and pathological findings. *Diagn Interv Radiol* 2011; 17:38–43

64. Rouvière O, Valette O, Grivolat S, et al. Recurrent prostate cancer after external beam radiotherapy: value of contrast-enhanced dynamic MRI in localizing intraprostatic tumor–correlation with biopsy findings. *Urology* 2004; 63:922–927

65. Pucar D, Hricak H, Shukla-Dave A, et al. Clinically significant prostate cancer local recurrence after radiation therapy occurs at the site of primary tumor: magnetic resonance imaging and step-section pathology evidence. *Int J Radiat Oncol Biol Phys* 2007; 69:62–69

66. Kim CK, Park BK, Lee HM, Kim SS, Kim E. MRI techniques for prediction of local tumor progression after high-intensity focused ultrasonic ablation of prostate cancer. *AJR* 2008; 190:1180–1186

67. Padhani AR, Khoo VS, Suckling J, Husband JE, Leach MO, Dearnaley DP. Evaluating the effect of rectal distension and rectal movement on prostate gland position using cine MRI. *Int J Radiat Oncol Biol Phys* 1999; 44:525–533